ELSEVIER

Catalysis Today 23 (1995) 251–267

CATALYSIS TODAY

Physical characterization of molybdenum oxycarbide catalyst; TEM, XRD and XPS

Pascale Delporte [a], Frédéric Meunier [a], Cuong Pham-Huu [a], Philippe Vennegues [b], Marc J. Ledoux [a,*], Jean Guille [c]

[a] *Laboratoire de Chimie des Matériaux Catalytiques, EHICS-ULP, 1 rue Blaise Pascal, 67000 Strasbourg, France*

[b] *CRHEA, Parc de Sophia Antipolis, Rue Bernard Gregory, 06570 Valbonne, France*

[c] *GEMME, IPCMS, EHICS-ULP, UMR46 CNRS, 23 rue du Loess, 67037 Strasbourg, France*

Abstract

Controlled reduction of MoO_3 can produce different phases of catalytic interest. One of these phases has been considered as being an oxycarbide of molybdenum. Various techniques mainly TEM but also XRD and others have been extensively used to understand the mechanism of formation and the structure of this oxycarbide. Its structure is reminiscent of the MoO_3 structure as shown by XRD, but reconstructed by shear planes and the introduction of carbon atoms to fill oxygen vacancies, both blocking the formation of MoO_2 the normal product of the slow reduction of MoO_3. The HRTEM pictures showed a 'chevron-like' arrangement and the electronic microdiffraction a square lattice reminiscent of the (0*k*0) planes of MoO_3.

1. Introduction

Since the first experimental results obtained by Boudart and Levy [1], several other publications [2,3] have illustrated the ability of metallic carbides to catalyze many chemical reactions. A large volume of literature [4–6] emphasizes the importance of the synthetic methods used to obtain products with high specific surface areas. Recently, both the work of Iglesia and coworkers [7–10] and that of our own group [11,12], have brought to light a new problem, linked to the activation process of the carbidic phases, the role of an oxidizing treatment (by air or oxygen) on the activity and the selectivity of these new catalysts.

The introduction of small quantities of oxygen on the 'clean' surface of tungsten carbide has, following Iglesia and coworkers [7], deeply modified the selectivity of this carbide for the isomerization reaction of saturated hydrocarbons, at the expense of the cracking reactions. An extensive study by CO and NH_3 chemisorption and by the use of many different reactive molecules [7–9] has led these authors to propose a reaction mechanism of the conventional bifunctional type, with dehydrogenation–hydrogenation steps on sites with a metallic character and steps of isomerization on sites of acidic type. However it should be stressed that in spite of the large amount of work carried out by this group, very few physical characterizations of the materials (other than chemisorption and BET) confirm the chemical results; in addition no reaction under flow allowing the evolution of the surface to be followed has been published. Finally, without it being explicitly expressed, this team seems to favor a surface of

* Corresponding author.

SSDI 0920-5861(94)00166-9

Table 1
n-Hexane isomerization at iso-conversion over oxicarbides prepared from different precursors. Reaction conditions: 350°C, 5 Torr n-C_6 partial pressure, 1 atm total pressure

Origin of catalysts	Metal	Carbide	Oxide
Time under flow (h)	24.75	25.5	17
Total flow (cm^3/min)	40	40	100
Conversion (%)	24.1	23	23.6
Rate (10^{-10} mol/g·s)	6349	9167	139850
Selectivity C_6 (%)	95	93	92.5
Total cracked (%)	5	7	7.5
Selectivity for the products of the reaction (% mol)			
Dimethyl-2,2 and 2,3 butane	1	1.2	1.3
Methyl-2 pentane	63	63.6	61.1
Methyl-3 pentane	35.2	34.4	36.9
Methylcyclopentane	0.6	0.4	0.4
Benzene + cyclohexane	0.2	0.4	0.3
$C_5 + C_1$	29	26	22.8
$C_4 + C_2$	34.7	25.6	34.4
$2C_3$	34	40.1	40
$3C_2$	1.4	4.1	2.1
$6C_1$	0.9	4.2	0.7

an heterogeneous nature: regions or sites of metallic character on one side, adsorbed oxygen or even surface oxide on the other side.

The catalytic results obtained by our group on molybdenum carbide submitted to an oxidizing treatment at 350°C for several hours, followed by an activation period under reactional flow (hydrocarbon + H_2), exhibit a great difference in activity and selectivity of saturated hydrocarbon reactions [11] when compared to the results obtained on 'clean' carbide surfaces [13]. The cracking reactions strongly diminished (from 90% to about 10%) to the benefit of chain isomerization without cyclization (more than 90%). In addition, the measured activity in terms of specific rate increased by a factor of 10, which gives, combined with the selectivity, a 100-fold increase in the yield of the isomer molecules. Later, it was shown that the same catalyst was able to isomerize n-C_7 in branched isomers with high activity and very high selectivity (>90%) at high conversion (80%), an impossible reaction on conventional bifunctional Pt/zeolite catalysts [14]. This activity bonus and this very high selectivity were due to the intervention of a non-bifunctional mechanism involving a metallacyclobutane intermediate [11,14] which might be due to the existence of a new, very active phase, molybdenum oxycarbide. But the presence of several amorphous or poorly crystallized phases proved by TEM (encapsulated charcoal, carbidic or oxicarbidic phases), makes the crystallographic analyses which would enable an easy characterization extremely complicated.

Fortunately, it has been possible to prepare an active phase with strictly identical selectivity properties, by starting either from MoO_3 or Mo metal instead of Mo_2C [15] (Table 1). To obtain this phase, it was necessary to superficially oxidize the metal foil and to treat this oxidized foil or the MoO_3 oxide with the reductive mixture hydrocarbon–hydrogen at 350°C for rather a long time (several hours), depending on the engaged mass of oxide and the characteristics of the flow.

The aim of this article is the study of the mechanism of transformation of MoO_3 into Mo oxycarbide mainly by HRTEM, but also using XRD and XPS, and ultimately to give the crystallographic structure of this oxycarbide.

2. Experimental

2.1. Products

MoO_3 (Strem Chemicals, 99.95% purity) was characterized by X-ray diffraction (XRD), which only showed the diffraction lines corresponding to the lattice parameters given by the JCPDS No. 5-508, $a = 3.963$ Å, $b = 13.855$ Å and $c = 3.696$ Å [43]. The metal foil Goodfellow 99.99% was 0.25 mm thick.

2.2. Analytical techniques

XRD was performed on a Siemens D-500 diffractometer with monochromatized radiation Co $K\alpha_1$ ($\lambda = 1.78901$ Å). The high-resolution transmission electronic microscopy (HRTEM) was carried out with a Topcon EM-002 B microscope working at 200 kV. The point-to-point resolution of this equipment could reach 1.8 Å. The samples

were ground and deposited on a copper grid covered by a carbon membrane, transparent to electrons and able to withstand the beam energy. The scanning electronic microscopy (SEM) was made on a JEOL JMS840 microscope. The samples deposited on a brass support were covered by a thin coat of gold to avoid the charge effect. XPS analyzes were performed in a Cameca Nanoscan-50 spectrometer using an X-ray source of Al Kα (1486.6 eV). The binding energies were calculated by taking the energy of the C 1s photoelectron at 284.8 $\pm$ 0.2 eV relative to the Fermi level. Only C 1s, O 1s and Mo 3d were recorded, and for a given emission the number of accumulations was selected in order to achieve a good signal-to-noise ratio. The samples were kept in the sealed reactor which was opened in a glove-box under a nitrogen atmosphere and then transferred onto the sample holder. Enclosed in a vessel, the mounted sample was transported to the spectrometer where it was transferred inside the XPS apparatus under flowing argon. The peak fit conditions used were: FWHM for metal = 1.0 eV and for oxide = 1.6 eV, ratio $3d_{5/2}/3d_{3/2} = 1.5$ and distance $3d_{5/2}$–$3d_{3/2}$ = 3.2 eV.

3. Results

3.1. Initial MoO_3

The BET surface of MoO_3 was 4 m^2/g. Its XRD diagram, shown in Fig. 1a, exhibits anomalously high intensities for all the $\langle 0k0 \rangle$ MoO_3 reflections. This is due to the structure of MoO_3 formed by layers of octahedra stacked along the [010] direction which favors platelet crystallites with a preferential orientation along this axis. This morphology is well illustrated by the low resolution TEM picture in Fig. 2a, where a platelet has dimensions of 0.7×0.15 μm^2 along the direction [100] and [001]. The SEM picture (Fig. 12a) also very well illustrates this platelet macroscopic shape. Under high resolution conditions the picture (Fig. 2b) shows a crystalline structure only over a short distance, but this was due to the high

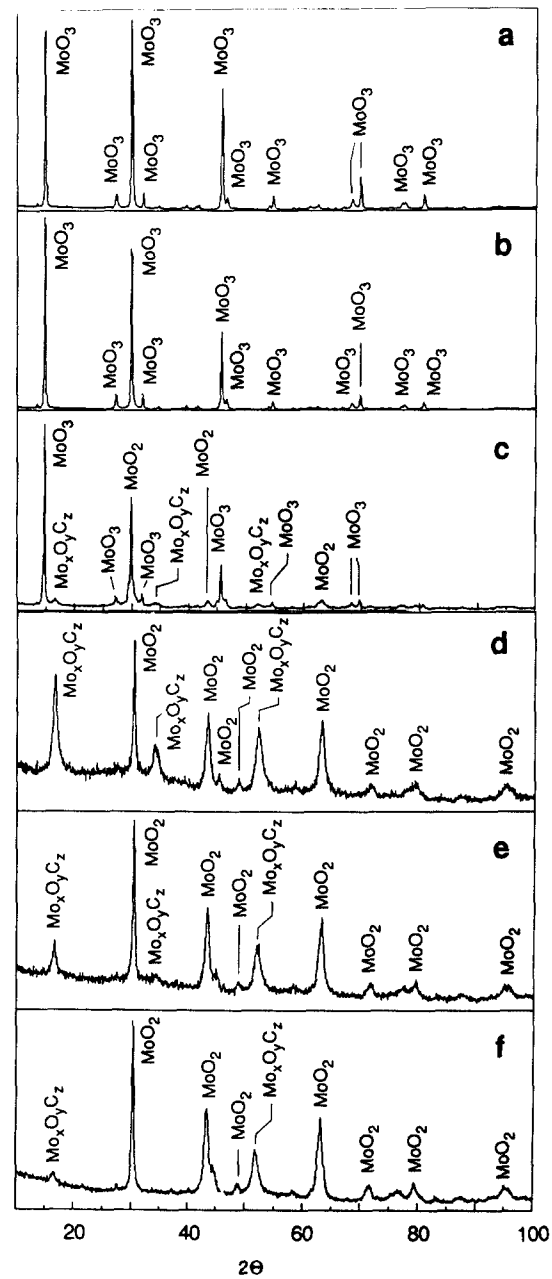

Fig. 1. X-ray powder diffraction pattern of MoO_3 after treatment at different times under H_2/n-C_6.

sensitivity of the sample under the beam. MoO_3 is one of the metal oxides which is known for its inability to preserve random distributed anionic defects and to form shear structures. The electronic microdiffraction carried out on these grains, submitted to a lower current, gives the lattice parameters $a = 3.95$ Å, $b = 13.8$ Å and $c = 3.65$ Å

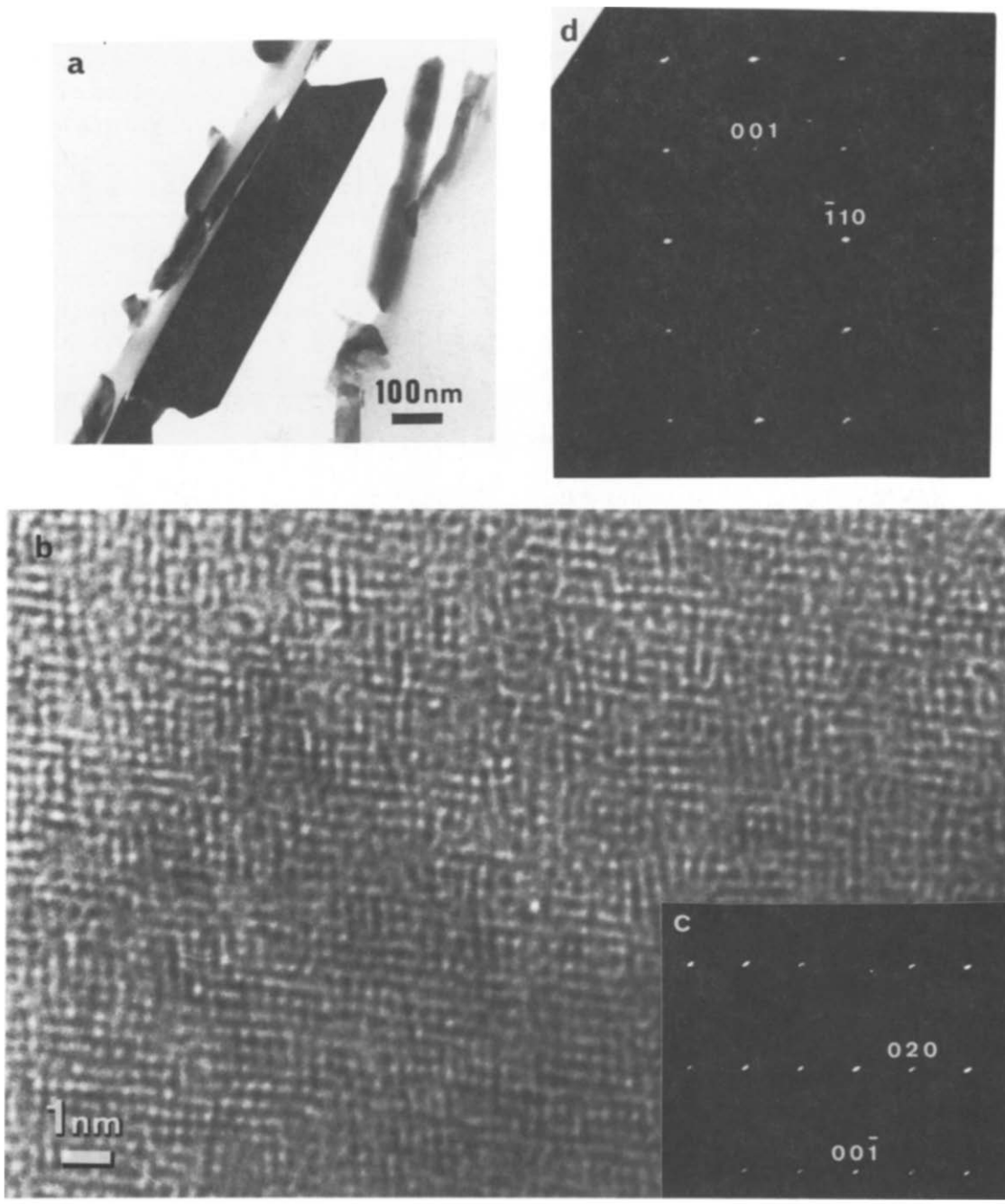

Fig. 2. (a) Low magnification micrograph of MoO_3 platelet. (b) HRTEM micrograph of (010) MoO_3 planes. (c) Selected area diffraction pattern of $[100]_{MoO_3}$. (d) Selected area diffraction of $[110]_{MoO_3}$.

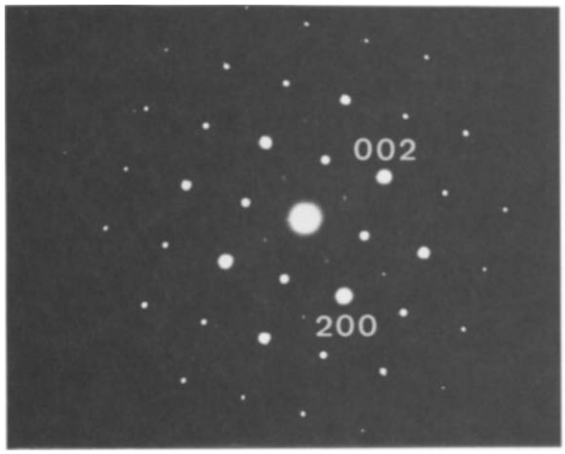

Fig. 3. Selected area diffraction pattern of $[010]_{MoO_3}$ after 1 h of treatment.

(Fig. 2c and d), which perfectly fit the parameters given by the literature.

3.2. MoO_3 after 1 h under n-hexane/hydrogen at 350°C

The sample was treated for 1 h under a flow of n-hexane/hydrogen at 350°C, and cooled down to room temperature under pure hydrogen flow. The XRD diagram (Fig. 1b) does not show any change when compared to the initial MoO_3. However, the color of the sample went from very pale blue to dark blue, indicating that at least a superficial reduction occurred during this first hour of treatment, and the specific surface area increased from 4 to 11 m^2/g. Something happened to the sample but on too thin a layer to be detected by XRD. The low resolution TEM analysis did not indicate any

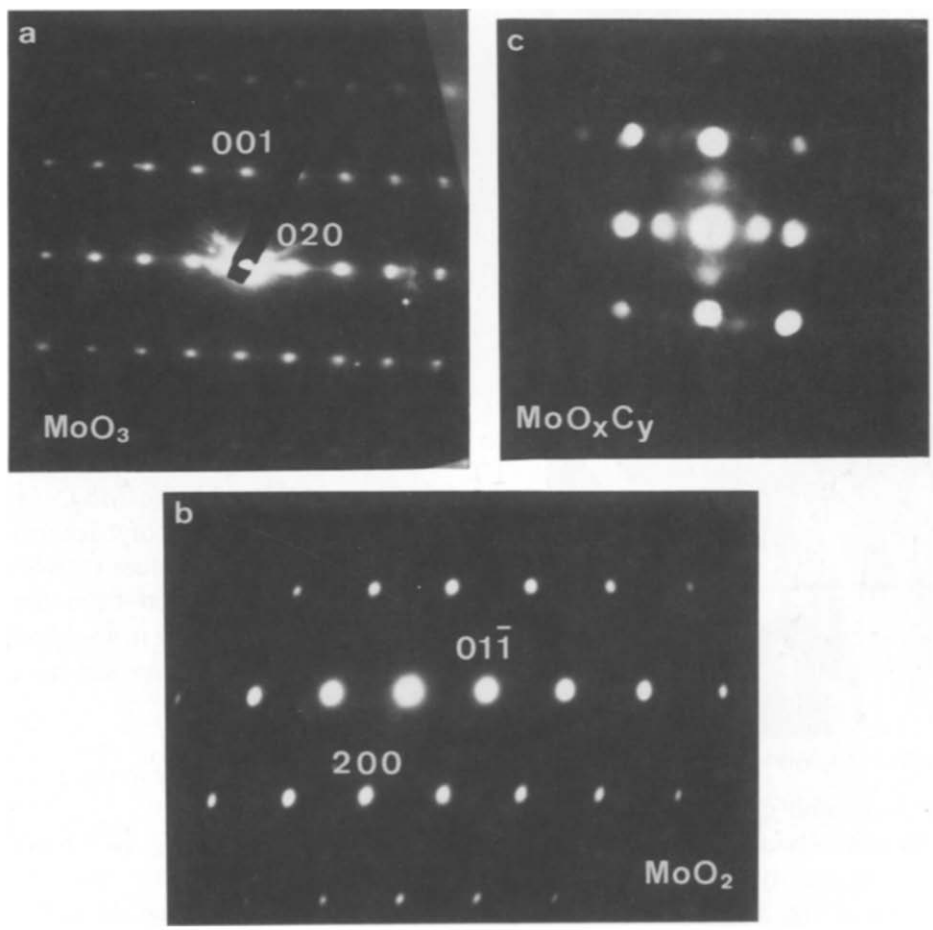

Fig. 4. (a) Selected area diffraction pattern of $[001]_{MoO_3}$ after 2 h of treatment. (b) $[011]_{MoO_2}$. (c) MoO_xC_y.

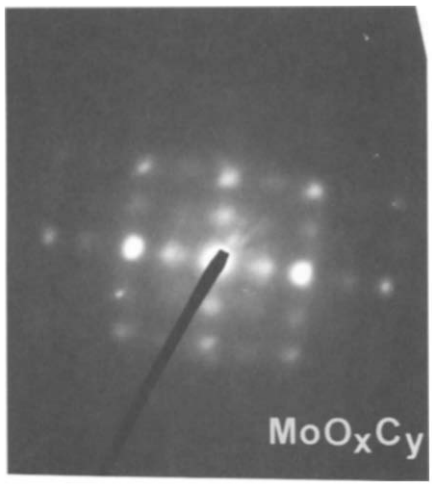

Fig. 5. Selected area diffraction pattern of MoO_xC_y after 3 h of treatment.

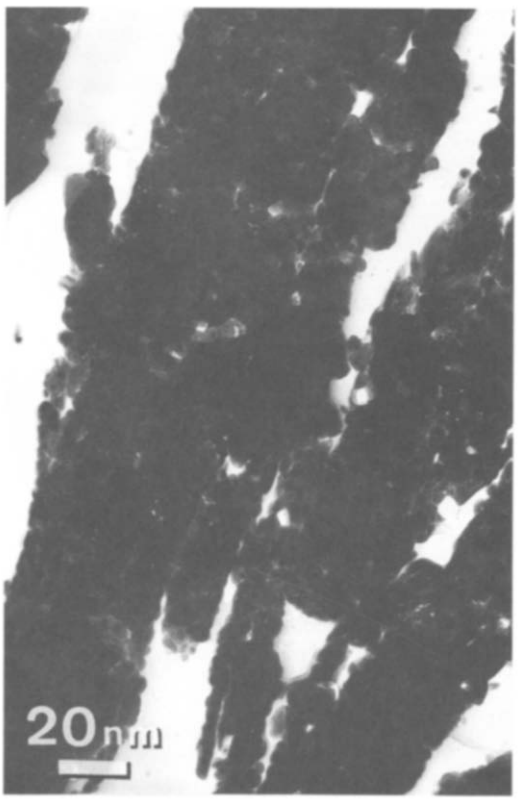

Fig. 6. Low magnification micrograph of MoO_3 after 7 h of treatment.

apparent micro-structural changes but the electronic microdiffraction (because it gives access to small grains coming mainly from the surface of the sample) shown in Fig. 3, along the zone axis [010] MoO_3, revealed spots normally forbidden for the group symmetry of MoO_3 ([h00] and [00l] with even h, l). This came from the modification of the surface and near surface symmetry due to the formation of oxygen vacancies by the reducing treatment. When a certain concentration of these vacancies was reached, they could be ordered in such a way that they formed a superlattice [16] thus allowing the appearance of the new spots. The HRTEM pictures were unable to show any changes when compared to the initial MoO_3 because a large amount of this product is still MoO_3 and remains unstable under the beam.

3.3. MoO_3 after 2 h of treatment

After 2 h under flow, the XRD diagram obtained from the sample (Fig. 1c) indicates the appearance of two new phases apart from MoO_3; MoO_2 and a new unknown phase which does not correspond to any analyzed by XRD and reported in the literature. Three weak peaks of this new phase can be observed at 2.05 Å, 4.1 Å and 6.2 Å when the 2θ angles are converted into inter-plane distances. For the sake of clarity, this new phase will be denoted as MoO_xC_y, in anticipation of the final result of this article which shows that this new phase is an oxycarbide of molybdenum.

The electronic microdiffraction performed on this sample shows the presence of MoO_3 domain (Fig. 4a), of MoO_2 domain (Fig. 4b) and diffraction patterns (Fig. 4c) which cannot be assigned to any phase susceptible to be formed by such a treatment (MoO_3, MoO_2, Mo_2C or any other known under-oxide of molybdenum). The only information on the structure of this new phase which could be obtained from the electronic microdiffraction, was that in one crystallographic plane the structure is square and has a parameter of 4.0 ± 0.1 Å.

3.4. MoO_3 after 3 h of treatment

The XRD diagram (Fig. 1d) shows that MoO_3 has completely disappeared from the sample to the benefit of MoO_2 and MoO_xC_y which are detected at much higher amounts than after 2 h of

treatment. The crystallographic planes corresponding to the three main peaks of MoO_xC_y are equidistant (2.05, 4.1 and 6.2 Å), which means that they belong to the same family and this distance is equivalent to the distance separating the $\langle 0k0 \rangle$ planes of MoO_3 but contracted by 14%. This indicates that the planes of MoO_xC_y are reminiscent of the MoO_3 planes. No other phases are detected. Electronic microdiffraction patterns again show the presence of MoO_2 (not presented here) and MoO_xC_y (Fig. 5). The specific surface area now reaches 49 m^2/g indicating an intensive destruction of the initial structure.

3.5. MoO_3 after 7 h of treatment

The XRD diagram of this sample (Fig. 1e) shows the presence of the same two phases as after 3 h — i.e. MoO_2 and MoO_xC_y. However, it should be stressed that the two peaks corresponding to the long distance order (4.1 and 6.2 Å) are disappearing from the diagram while the short-range

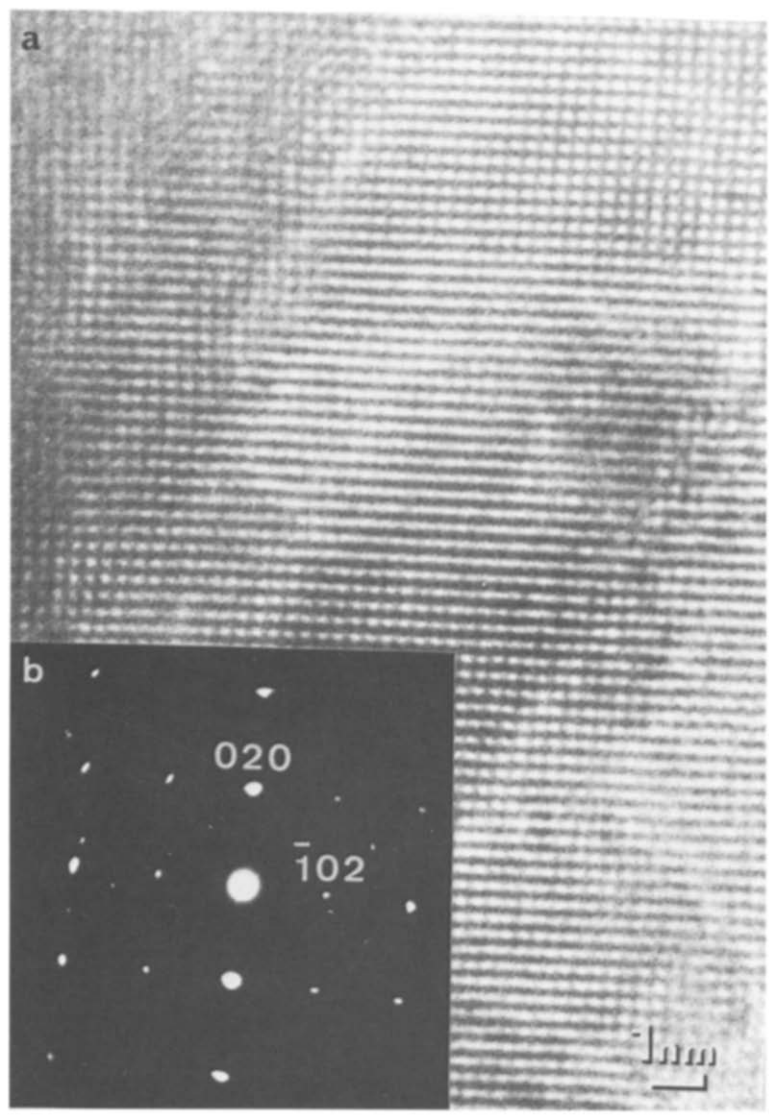

Fig. 7. (a) HRTEM micrograph of (100) MoO_2 planes after 7 h of treatment. (b) Selected area diffraction pattern of $[100]_{MoO_2}$.

order (2.05 Å) is hardly affected. This evolution was even more accentuated after 53 h of treatment (Fig. 1f) where the two peaks at 4.1 and 6.2 Å were almost not detected. The same consequent destruction of this initial long-range order was also observed by electron microdiffraction where the spots corresponding to the 4.1 Å distance (Fig. 4c) almost disappeared from the picture (Fig. 8b). This evolution also affected the specific surface area which reached 147 m^2/g after 7 h then to remain stable. The low resolution TEM made after 7 h (Fig. 6) shows an obvious change in the macroscopic aspect of the crystallite. In Fig. 2a, it is shown that the starting MoO_3 crystallites were in platelet shape without apparent microdefects. In Fig. 6 the same platelet shapes are now totally divided into small domains. The HRTEM pictures indicate the presence of well organized MoO_2 which is confirmed by electronic microdiffraction (Fig. 7b) and a structure in a 'chevron' shape and the corresponding electronic microdiffraction (Fig. 8b), characteristic of MoO_xC_y. These two

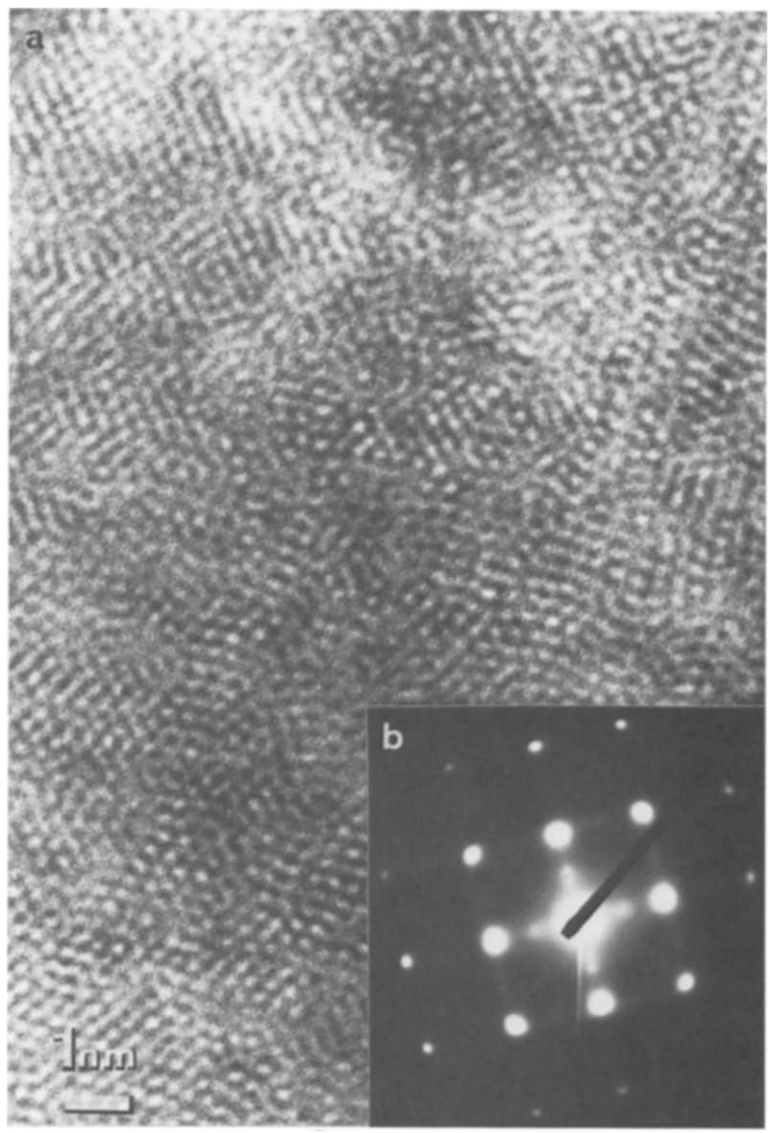

Fig. 8. (a) HRTEM micrograph of MoO_xC_y after 7 h of treatment. (b) Selected area diffraction pattern of MoO_xC_y.

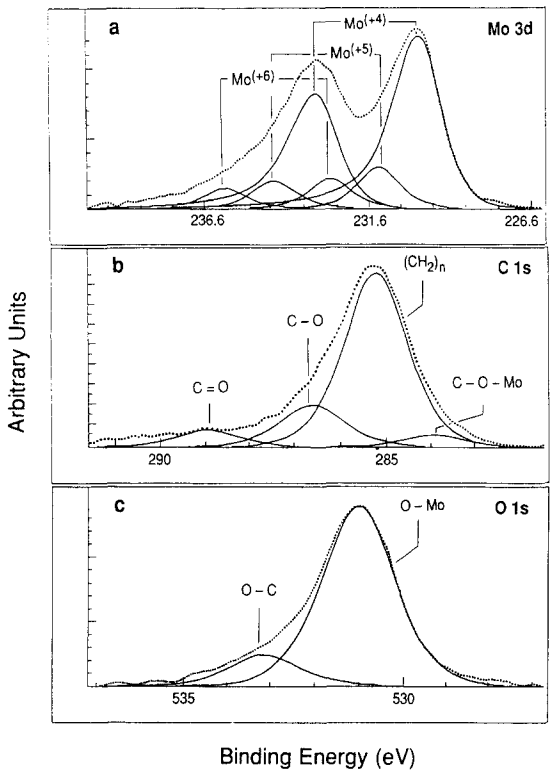

Fig. 9. XPS of activated Mo foil.

structures are more stable under the electron beam than MoO_3 because no deterioration of the sample was ever observed during observation.

3.6. *XPS analysis of the sample after 7 h of treatment*

Because of the difficulty in analyzing samples prepared either from Mo_2C (carbide route) or from MoO_3 (oxide route) due to the charge effect, it was decided to try to prepare MoO_xC_y from metal foil. A superficial oxidation of the surface into MoO_3 followed by the reducing treatment under n-hexane/hydrogen flow led to a surface with the same high selectivity patterns in the reaction of isomerization of n-C_6 (see Table 1). It was thus assumed that the upper layer of the sample was the same MoO_xC_y phase than the one prepared by the two other routes. The analyses of the clean or oxidized Mo foil were done but are not reported here. The oxidized foil only exhibited the doublet Mo 3d of Mo^{6+}, situated 5 eV higher in binding energy than the peak representing the metal state as already reported by several authors [17–19]. The molybdenum oxide peaks were symmetrical, with the FWHM of Mo $3d_{5/2}$ equal to 1.4 eV and the Mo $3d_{5/2}$ and $3d_{3/2}$ located at 232.6 and 235.8 eV respectively [13,20,21]. A small amount of Mo^{5+} located at 230.4 eV according to the data reported in the literature [22] was also observed. The corresponding O 1s signal was also perfectly symmetrical and located at 530.7 eV. This indicated that only one type of lattice oxygen was present in the different molybdenum oxides in agreement with the results published by Haber et al. [23].

The activated sample showed that the Mo 3d doublet contains mainly Mo^{4+} and Mo^{5+} with a small amount of Mo^{6+} (Fig. 9a) with the $3d_{5/2}$ bands respectively located at 229.7, 230.8 and 232.5 eV. No peak corresponding to Mo carbide [12] or Mo metal could be detected. 85% of the signal was due to the Mo^{4+} state. Examination of the C 1s and O 1s high resolution spectra (Fig. 9b and c) shows that the Mo^{4+} state is not only due to MoO_2 but also to another phase. Four overlapping XPS peaks could be deconvoluted from the broad recorded C 1s peak. The peak at 284.8 eV (285.2 eV on the non-corrected spectrum) was attributed to amorphous carbon or to adsorbed hydrocarbon as reported by several authors [24,25]. The peaks at 286.2 and 288.5 eV were attributed to the carbon atoms involved in carbonate species (C–O and C=O, respectively) according to the literature [26]. The small peak observed at 283.5 eV could correspond to a carbon bonded to oxygen and metal in an oxycarbide form at 1.2 eV higher than in the carbide form, in agreement with several publications dealing either with silicon oxycarbide [27,28] or aluminium oxycarbide [26]. Very close binding energies to those observed here were reported by Julbe et al. [29] studying silicon oxycarbide; 284.4 eV for contaminating carbon against 284.8 eV here and 282.7 eV for Si–C in the carbide against 282.8 eV for Mo–C in the carbide, with the oxycarbide peak located between these two limits, 283.2 eV for silicon oxycarbide and 283.5 eV here.

The O 1s XPS spectrum also showed the presence of more than one peak. The peak located at 530.6 eV was attributed to oxygen bonded to metal. But because the chemical shift observed for the oxygen peak is small, it is difficult to ascertain the occurrence of a new peak by deconvolution analysis. The symmetrical second O 1s peak at 532.7 eV was attributed to O atoms in the carbonate species.

4. Discussion

4.1. Crystallographic structure of MoO_3 and MoO_2

The crystallographic structure of MoO_3 is presented in Fig. 10; it belongs to the orthorhombic system Pnma ($a=3.69$ Å, $b=13.86$ Å and $c=3.69$ Å) [30]. It is a layered structure where each layer is made of two half-layers of MoO_6 octahedra slightly distorted [31]. The successive layers, parallel to the plane (010), are linked via Van der Waals forces. Within a half-layer the octahedra are connected by common corners along the axes [100] and [001] and between each half-layer they are connected by common edges. The relative position of one layer and its first neighbor is such that the oxygen atoms bonded to a single Mo atom and pointing along [010], are located below (or above) and between two oxygen atoms of the same type of the next layer.

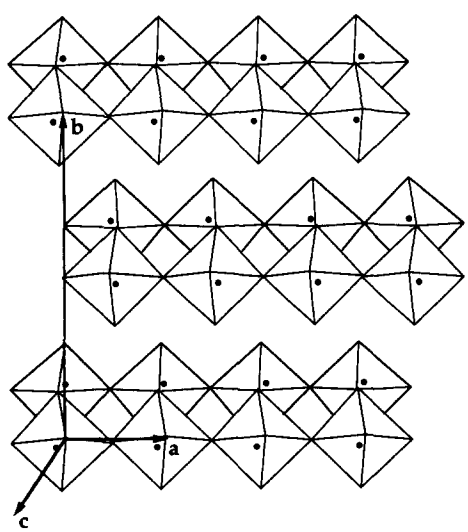

Fig. 10. Crystalline structure of MoO_3.

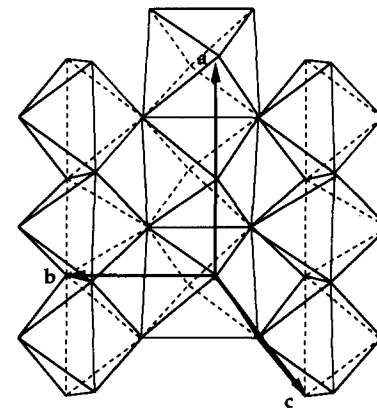

Fig. 11. Crystalline structure of MoO_2.

The crystallographic structure of MoO_2 is presented in Fig. 11; it belongs to the monoclinic system with parameters such as $a=5.61$ Å, $b=4.85$ Å, $c=5.63$ Å and $\beta=120°57$ [32,33]. This structure is made of MoO_6 octahedra, only very slightly distorted, which are sharing edges to form strings. These strings are mutually connected to a 3-D structure by octahedra sharing corners.

4.2. Nature of the transformation of MoO_3 into MoO_2 and MoO_xC_y

MoO_3 has, as shown above, a macroscopic platelet shape with a very smooth surface aspect as confirmed by the SEM pictures (Fig. 12a); after the reducing treatment under n-C_6/H_2, the surface is becoming rough (Fig. 12b) but the macroscopic shape of the crystallites (platelets) is maintained. These observations mean that the transformation under 'soft' conditions of treatment is topotactic by preserving a preferential plane, $\langle 0k0 \rangle$ [34].

4.3. Mechanism of the transformation

4.3.1. First step

The slow reduction at 350°C starts from the surface as shown by the sample after 1 h of treatment. The formation of surface oxygen vacancies

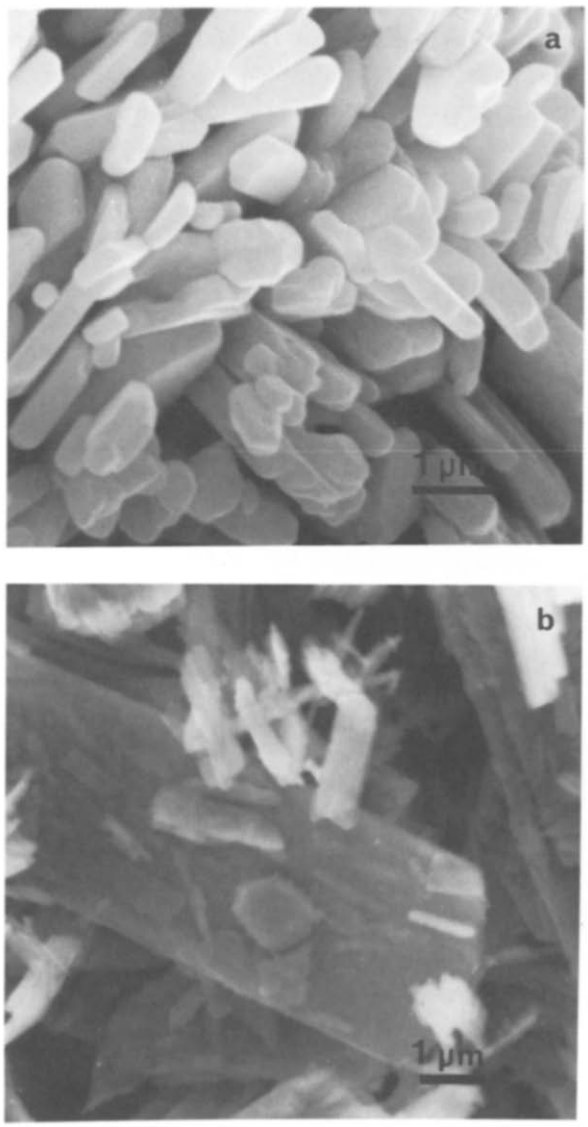

Fig. 12. SEM micrographs of (a) MoO_3 and (b) MoO_3 after 7 h under H_2/n-C6.

has already been studied [16,23,35] and can be summarized as follows:

Hydrogen adsorption on the (010) plane, i.e. on the oxygen atoms bonded to a single Mo atom (because of the layered structure).

Water elimination from two adjacent OH groups.

$$OH + OH \rightarrow H_2O + O_{lattice} + \square$$

These vacancies can be randomly distributed in the plane (010) and if the reaction stops here the surface can easily re-arrange by the intermediate of shear planes [36]. But a deeper and longer reduction produces a higher concentration of vacancies which will re-organize themselves along [101] (see Fig. 13) because it is the most energetically favourable situation [36] with each octahedron bearing a vacancy surrounded by saturated octahedra.

4.3.2. Second step

As oxygen is removed during the initial stage of reduction, the MoO_3 lattice may rearrange to eliminate vacancies by local collapse and shear along $\pm 1/2a + 1/7b$ in the $(120)_{MoO_3}$ plane, as described by Bursill. Consequently, there is a decrease of the [010] distance. From this intermediate state and depending on the nature and the composition of the reducing flow, two products can be formed, either MoO_2 or, by integration of carbon atoms present in the flow, the oxycarbide phase MoO_xC_y.

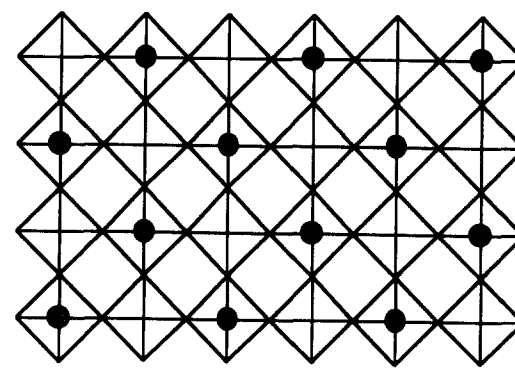

Fig. 13. Re-organization of oxygen vacancies in the (010) plane of MoO_3.

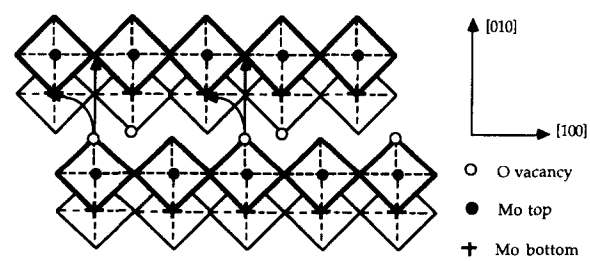

Fig. 14. Re-organization of the layers in the (001) plane.

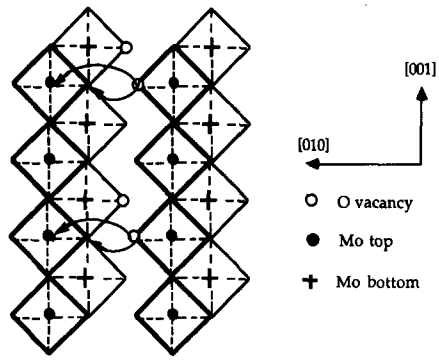

Fig. 15. Re-organization of the layers in the (100) plane.

4.3.3. MoO_3 to MoO_2

The reduction in the distance between the (010) planes allows the oxygen vacancies formed during the first step to be filled. For the sake of clarity, it is necessary to illustrate the crystallographic mechanism by schematic figures. Figs. 14 and Fig. 15 show two consecutive layers of MoO_3 along [010], $z=0$ and $z=b/2$, separated by the Van der Waals void, each layer contains two half-layers of octahedra. The oxygen vacancies shown as circles can easily be filled by oxygen atoms from the nearest plane $b/2$. Since the octahedra are distorted ($a \neq c$ and O–Mo–O $\neq 180°$), the movements are not fully symmetrical but a reorganization in the octahedra planes (tilts and distortions) leads directly to MoO_2, a stable phase which does not evolve with time on stream. This rearrangement is a cooperative movement: all octahedra move at the same time, which leads to a MoO_2 phase with big crystallites, which are observed on the HRTEM image.

4.3.4. MoO_3 to MoO_xC_y

In parallel with the removal of the oxygen vacancies with MoO_2 formation, the first step leads to the formation of shear planes, and, when the process carries on and at a sufficiently high concentration of defects, the lattice collapses: the parameter along [010] is contracted by 14% (measured by microdiffraction and XRD). Thus, instead of a stable structure, a carbon–oxygen substitution can occur because of the nature of the flow; the reduction under the mixture hydrocarbon/hydrogen can introduce carbon atoms during the process and stabilize the intermediate phase. Indeed, Spevack and McIntyre [36] considered, through the study of H_2S reacting on MoO_3 films, that these shear planes are the preferential pathways for diffusion of sulfur atoms to form molybdenum oxysulfide because they represent lines of high lattice energy between two MoO_2 stable but mismatched phases. In the same way, one can imagine that carbon can act like sulfur atoms to form the MoO_xC_y oxycarbide phase.

The time required for catalytic activation corresponds to oxygen substitution by carbon, with a progressive narrowing of the gap between the layers by shear. When the phase is in equilibrium (i.e. no more substitution) and when the catalytic steady state is reached, the new crystalline phase MoO_xC_y is obtained; the XRD peaks of the orthorhombic structure at 4.1 and 6.2 Å disappear and the brightest spots on the negatives of microdiffraction are at 2.05 Å. This could correspond to a compact stacking of the initial octahedra leading to a pseudo-cubic structure; the height of one distorted octahedron of MoO_3 is equal to 3.94 Å; thus, by carbon/oxygen substitution and reorganization, a period of approximately 4.1 ± 0.1 Å is quite possible. The 4.1 Å distance corresponding

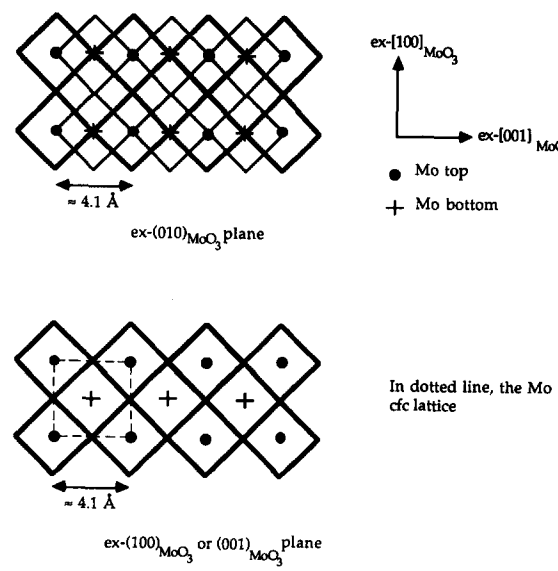

Fig. 16. Arrangement of Mo atoms and octahedra in an ex-layer.

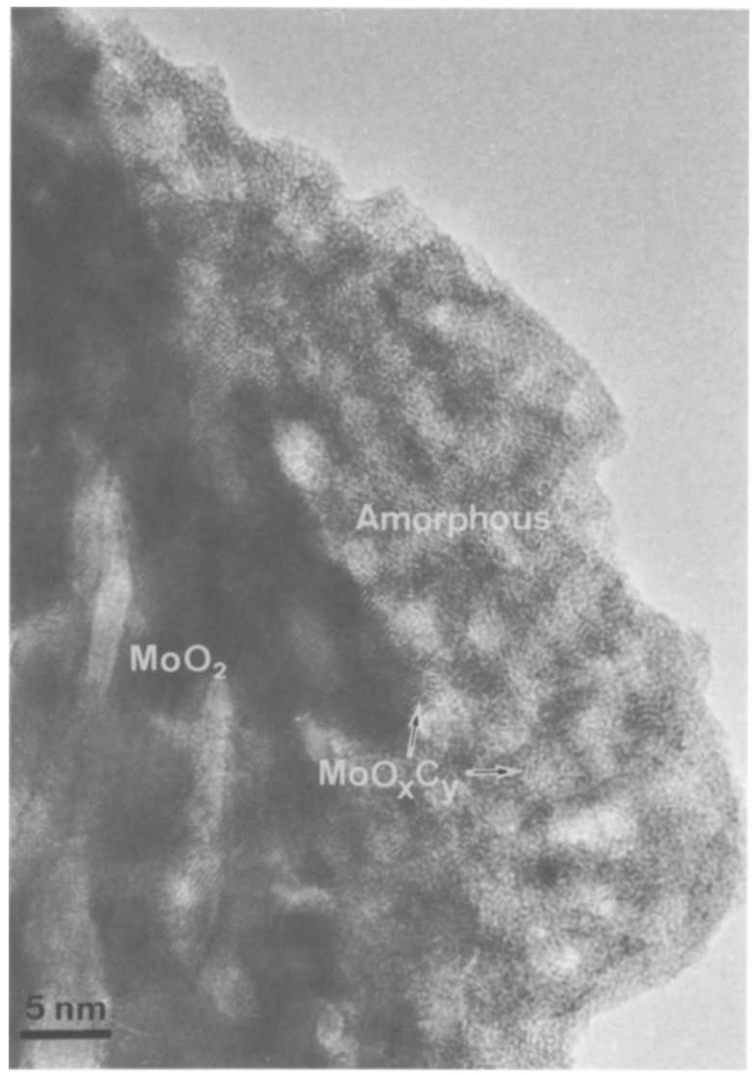

Fig. 17. HRTEM micrograph showing the co-existence of crystallized MoO_xC_y enbedded into its amorphous form.

to the (010) plane cannot be observed by diffraction because of the symmetry rule of a cubic structure and only diffraction corresponding to the (020) plane (2.05 Å) is observable. The pseudo-cubic arrangement is maintained in the ex-$(010)_{MoO_3}$ plane while a square lattice with centered Mo atoms is built in the ex-$(100)_{MoO_3}$ and $(001)_{MoO_3}$ planes (Fig. 16). Because of this peculiar structure, all the microdiffractions performed on the samples always show a square lattice structure. If for this new phase the shear does not occur in a cooperative way but in successive movements, only small ordered domains can be formed which would explain the 'chevron-like' structure observed on the HRTEM images and the broad spots on the microdiffraction pictures.

If the reorganization of the structure is too fast or not concerted because of the use of different values for the important parameters (hydrocarbon partial pressure, temperature, etc. ...), the final oxycarbide phase can be amorphous and not organized in small domains. The broadening of the XRD peaks is the first evidence of such a disorder (Fig. 1). Indeed in many cases such an amorphous phase was observed together with the 'chevron-like' structure as shown in Fig. 17. The

large increase in the surface during the formation of the oxycarbide could be partly interpreted by the presence of this amorphous phase.

This oxycarbide is very different from the MoO_xC_y prepared by decomposition of $Mo(CO)_6$ by Leclercq and coworkers [37,38]. The XRD patterns of their material exhibit four main peaks including a strong doublet at $2\theta \cong 38°$ and $2\theta \cong 43°$ (Cu Kα) [39]. This structure seems to be very close to the structure of the fcc Mo_2C (two peaks at $2\theta \cong 37°$ and $2\theta \cong 43°$ (Cu Kα)) or the fcc Mo_2N (two peaks at $2\theta \cong 37°$ and $2\theta \cong 44°$ (Cu Kα) measured by Ranhotra et al. [40]. The XRD patterns of the oxycarbide of the present study (Fig. 1) show two main peaks (reminiscent of the MoO_3 three main peaks) at $2\theta \cong 16.6°$ and $2\theta \cong 51.8°$ (Co Kα) corresponding to 9.1° and 44.3° respectively with Cu Kα. A strong reduction of this oxycarbide leads to the hcp Mo_2C, with one main peak at $2\theta \cong 39°$ (Cu Kα) [43].

The competitive nature of the two mechanism of the second step was further studied in experiments carried out under pure hydrogen reducing flow. In Fig. 18, the XRD diagrams of MoO_3 (Fig. 18a) reduced by pure hydrogen at 350°C for 7 and 11 h (Fig. 18b and c) show that after 7 h three phases were observed: MoO_2, $MoO_{2.5}OH_{0.5}$ and $MoO_x(H)_y$, after 11 h $MoO_{2.5}OH_{0.5}$ had disappeared. At 400°C (Fig. 18d) after 7 h only MoO_2 was observed with a trace of Mo metal while at 450°C and 15 h (Figs. 18e and 20) more metal was found. One can imagine that H or H_2 can act like C atoms to form a $MoO_x(H)_y$ phase. However because of the dimension and the electronic properties of the H radical or the H_2 molecule, the $MoO_x(H)_y$ species should be quite unstable compared to MoO_xC_y, where C atoms can fill the vacancies to block the process of reduction into MoO_2. The introduction of this H containing under-oxide of molybdenum is not necessary to explain and to prove the existence of the oxycarbide phase but it fits well with the different phenomena which occur during the complex process of reduction.

A reduction under the mixture n-C_6/H_2 can introduce carbon atoms during the process and

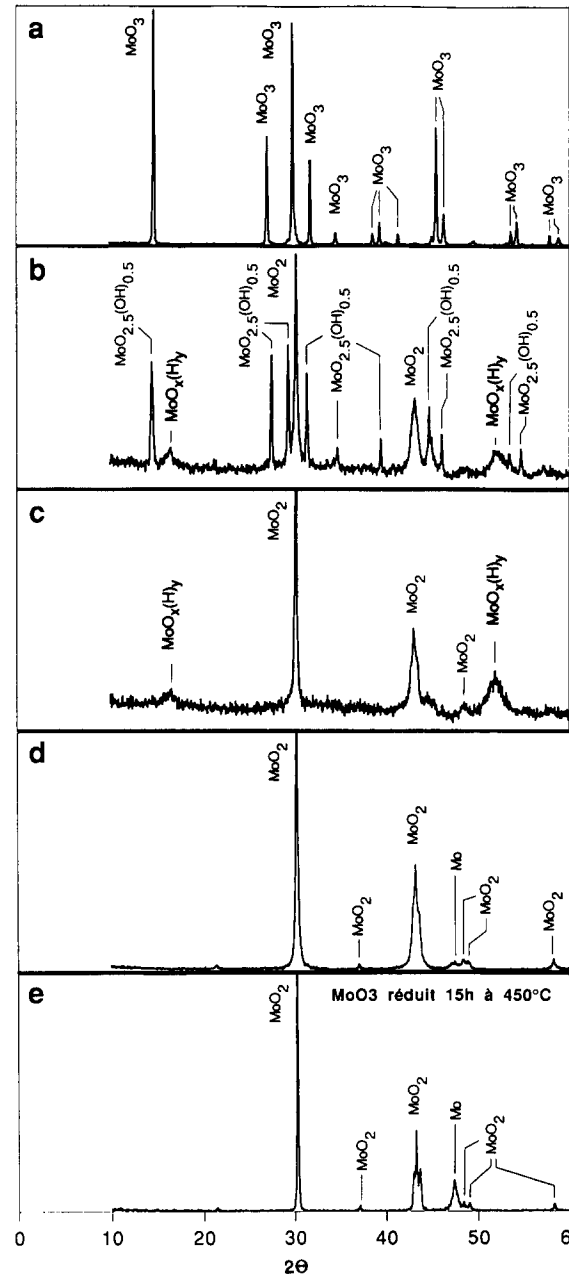

Fig. 18. X-ray powder diffraction pattern of MoO_3 after treatment at different times and temperatures under pure H_2.

stabilize the intermediate phase which was denoted as MoO_xC_y. This phase can also be obtained after reduction under pure hydrogen on condition that the $MoO_x(H)_y$ phase has not totally disappeared from the sample, because otherwise pure MoO_2 cannot evolve into MoO_xC_y (see Scheme 1). The fact that MoO_2 does not transform

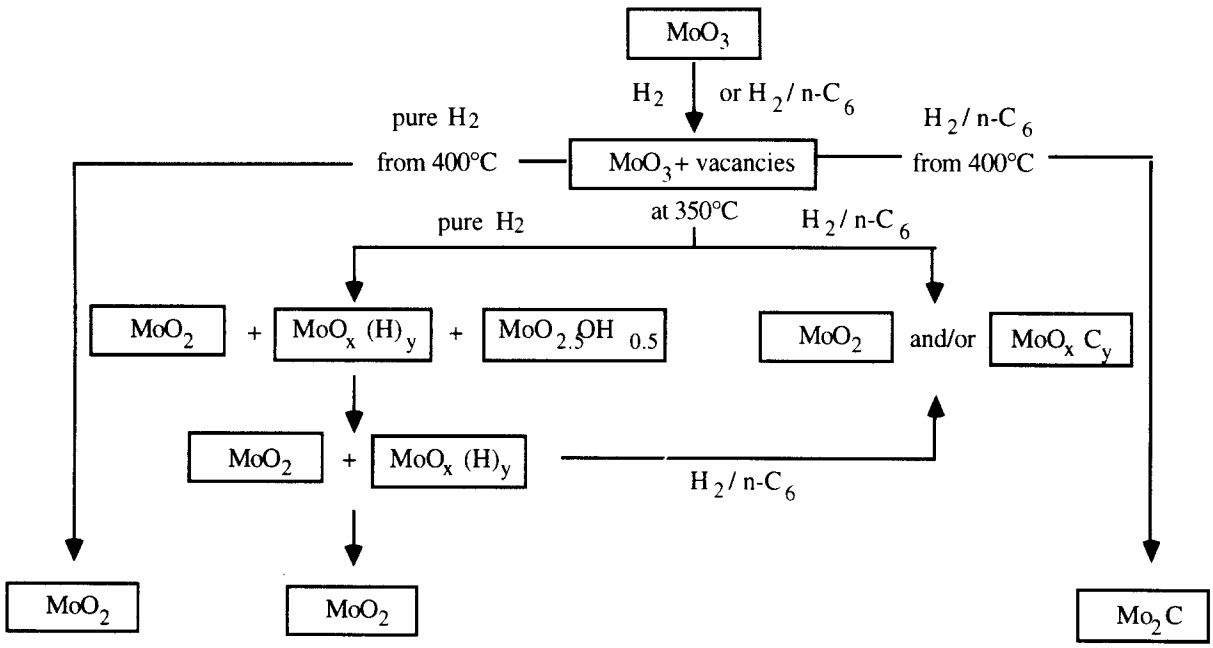

Scheme 1.

into MoO_xC_y well explains why it has always been impossible to have an active catalyst whatever the activation process when MoO_2 was used as starting material. In addition it was observed that after 7h of reduction under pure hydrogen, the amount of the $MoO_x(H)_y$ phase was decreasing to the benefit of MoO_2 and in turn the isomerization activity of the catalyst was following this decrease because not enough MoO_xC_y phase was produced. The parallel structural evolution when the reduction feed contains or does not contain hydrocarbon

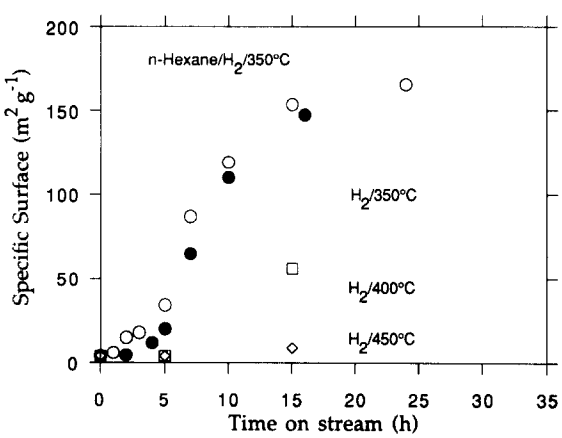

Fig. 19. BET surface area of MoO_3 after different treatments.

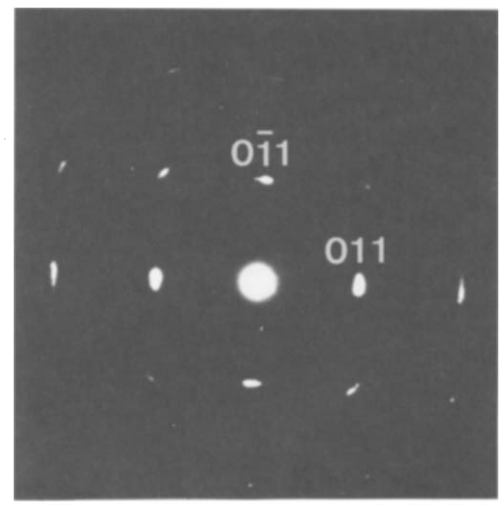

Fig. 20. Selected area diffraction pattern of $[201]_{MoO_2}$.

was also confirmed by the evolution of the specific surface area measured on the sample versus time of reduction (Fig. 19). At 350°C whatever the nature of the feed, the surface area increased from 4 to about 150 m^2/g; at 400°C and even more so at 450°C, under pure hydrogen, the surface hardly increased. The reduction at temperatures higher than 400°C under the mixture containing hydrocarbon and hydrogen led to molybdenum carbide,

the method used by Boudart et al. to prepare these carbides.

5. Conclusion

The formation of the MoO_xC_y phase from MoO_3 is now easier to understand: creation of oxygen vacancies on MoO_3 planes (010) accompanied by a contraction of the distance between the layers through shear planes which minimize the constraints and fill some vacancies. If the number of vacancies is too high, then the solid reconstructs into MoO_2. If carbon is added to the flow and on condition that the temperature is not too high (below 400°C), some carbon atoms stop the contraction of the planes at a level of 14% along [010]. The longer the reduction in the presence of carbon carries on, the larger is the amount of shear planes thus of oxycarbide, with a progressive destruction of long distance order to eventually reach only short distance order (disappearance of 6.2 and 4.1 Å distances between $\langle 0k0 \rangle$ planes), with the constitution of small shifted domains which show the 'chevron-like' structure. Electronic diffraction indicates that this phase has a square lattice, with a parameter equal to 4.1 ± 0.1 Å. This square lattice is due to the contraction of the Van der Waals gap which sticks together octahedra from both sides of the gap. But it has not been possible to go further in the determination of the exact structure because the transformation of MoO_3 involves distorted MoO_6 octahedra, containing or not containing carbon atoms, which make the simulation very complex to perform. An X-ray structure made from a single crystal will be probably the ultimate solution. In such a structure molybdenum atoms should be present mainly as Mo^{5+} and Mo^{4+}, which is exactly what XPS analyses performed on a thin layer of MoO_xC_y phase show. Preliminary experiments using ^{13}C MAS-NMR on different samples of the MoO_xC_y phase confirm the presence of carbon atoms in a totally different environment than in molybdenum carbide and will be published later [41,42].

Acknowledgements

This research was supported by the Péchiney Company. Gabrielle Ehret (IPCMS, Strasbourg) is gratefully acknowledged for her technical assistance.

References

[1] M. Boudart and R. Levy, Science, 181 (1973) 547.
[2] S.T. Oyama and G.L. Haller, Catalysis, Specialist Periodical Reports V5, Royal Chem. Soc. (London), (1982).
[3] M.J. Ledoux and C. Pham-Huu, Catal. Today, 15 (1992) 263.
[4] L. Volpe and M. Boudart, J. Solid State Chem., 59 (1985) 780.
[5] J.S. Lee and M. Boudart, Catal. Lett., 8 (1991) 107.
[6] M.J. Ledoux, J. Guille, C. Pham-Huu and S. Marin, Eur. Pat. Appl. 0 396 475 A1 (1989).
[7] F.H. Ribeiro, R.A. Dalla Betta, M. Boudart, J.E. Baumgartner and E. Iglesia, J. Catal., 130 (1991) 86.
[8] F.H. Ribeiro, M. Boudart, R.A. Dalla Betta and E. Iglesia, J. Catal., 130 (1991) 498.
[9] E. Iglesia, J.E. Baumgartner, F.H. Ribeiro and M. Boudart, J. Catal., 131 (1991) 523.
[10] E. Iglesia, F.H. Ribeiro, M. Boudart and J.E. Baumgartner, Catal. Today, 15 (1992) 307.
[11] M.J. Ledoux, C. Pham-Huu and J. Guille, J. Catal., 143 (1993) 249.
[12] M.J. Ledoux, C. Pham-Huu, H. Dunlop and J. Guille, in L. Guczi et al. (Editors), New Frontiers in Catalysis, 10th ICC, Akadémiai, Budapest, (1992) p. 955.
[13] M.J. Ledoux, C. Pham-Huu, H. Dunlop and J. Guille, J. Catal., 134 (1992) 383.
[14] E.A. Blekkan, C. Pham-Huu, M.J. Ledoux and J. Guille, Ind. Eng. Chem. Res., 33 (7) (1994) 1657.
[15] M.J. Ledoux, C. Pham-Huu, J. Guille and M. Prin, Eur. Pat. Appl. 91 12374
[16] L.A. Bursill, Proc. Roy. Soc. A, 311 (1969) 267.
[17] Y. Holl, R. Touroude, G. Maire, A. Muller, P.A. Engelhard and J. Grosmangin, J. Catal., 104 (1987) 202.
[18] T.H. Fleisch and G.J. Rains, J. Chem. Phys., 76 (1982) 780.
[19] R.L. Chin and D.M. Hercules, J. Phys. Chem., 86 (1982) 3079.
[20] I. Olefjord, B. Brox and U. Jelvestam, J. Electrochem. Soc., 132 (1985) 2854.
[21] J.E. De Vries, H.C. Yao, R.J. Baird and H.S. Gandhi, J. Catal., 84 (1983) 8.
[22] A. Cimino and B.A. De Angelis, J. Catal., 36 (1975) 11.
[23] J. Haber, W. Marczewski, J. Stoch and L. Ungier, Ber. Bunsen Gesellschaft Phys. Chem., 79 (1975) 970.
[24] L. Ramqvist, K. Mamrin, G. Johansson, A. Fahlman and C. Nordling, J. Phys. Chem. Solids, 30 (1969) 1835.
[25] D.R. Wheeler and S.V. Pepper, Surf. Inter. Anal., 10 (1987) 153.
[26] M. Bou, J.M. Martin, T. Le Mogne and L. Vovelle, Appl. Surf. Sci., 47 (1991) 149.
[27] L. Porte and A. Sartre, J. Mater. Sci., 24 (1989) 271.

[28] E. Bouillon, D. Mocaer, J.F. Villeneuve, R. Pailler, R. Naslain, M. Monthioux, A. Oberlin, C. Guimon and G. Pfister, J. Mater. Sci., 26 (1991) 1517.
[29] A. Julbe, A. Larbot, C. Guizard, L. Cot, T. Dupin, J. Charpin and P. Bergez, Eur. J. Solid State Inorg. Chem., 26 (1989) 101.
[30] G. Andersson and A. Magneli, Acta Chem. Scand., 4 (1950) 793.
[31] L. Kihlborg, Arkiv. Kem., 21 (1963) 357.
[32] G. Andersson and A. Magneli, Acta Chem. Scand., 9 (1955) 1378.
[33] B.G. Brandt and A.C. Skapski, Acta Chem. Scand., 21 (1967) 661.
[34] O. Bertrand and L.C. Dufour, Phys. Stat. Sol. (A), 60 (1980) 507.
[35] L.C. Dufour, O. Bertrand and N. Floquet, Surf. Sci., 147 (1984) 396.
[36] P.A. Spevack and N.S. McIntyre, J. Phys. Chem., 97 (1993) 11031.
[37] L. Leclercq, K. Imura, S. Yoshida, T. Barbee and M. Boudart, Stud. Surf. Sci. Catal., 3 (1979) 627.
[38] M. Boudart, S.T. Oyama and L. Leclercq, in T. Seiyafna and K. Tanabe (Editors), Proc. of the 7th ICC, Tokyo, Vol. 1, Elsevier, Amsterdam, 1980, p. 578.
[39] S.T. Oyama, PhD Dissertation, Stanford University, (1981) p. 24.
[40] G.S. Ranhotra, G.W. Haddix, A.T. Bell and J.A. Reimer, J. Catal., 108 (1987) 24.
[41] M.J. Ledoux, C. Pham-Huu, P. Delporte, E.A. Blekkan, A.P.E. York, E.G. Derouane and A. Fonseca, Proc. of TOCAT 2, Tokyo, (1994), in press.
[42] P. Delporte, to be published.
[43] Nat. Bur. of Stand. (US), Monogr. 25, 20 (1984) 118.